ISSN 1392–3730
JOURNAL OF CIVIL ENGINEERING AND MANAGEMENT
http:/www.vtu.lt/english/editions

2004, Vol X, No 3, 199–208

ADVANCED ANALYSIS OF STEEL FRAMES WITH EFFECTS OF JOINT DEFORMABILITY AND PARTIAL STRENGTH ACCOUNTED FOR

Marian A. Gizejowski[1], Czeslaw J. Branicki[2], Anna M. Barszcz[3], Pawel Krol[4]

[1,2]*University of Botswana, P. Bag 0061, Gaborobne, Botswana.* [1]*E-mail: gizej@mopipi.ub.bw,*
[2]*E-mail: branic@mopipi.ub.bw,* [3,4]*Warsaw University of Technology, Armii Ludowej 16, 00-637 Warsaw, Poland.*
[3]*E-mail: abar@il.pw.edu.pl,* [4]*E-mail: p.krol@ il.pw.edu.pl*

Received 1 Dec 2003; accepted 21 May 2004

Abstract. The paper summarises the current progress in methods of advanced analysis for design of frames with semi-rigid joints. The methods presented in the paper belong to general second-order refined plastic-hinge methods that allow for the combined effects of joint stiffness degradation and distributed plasticity along the member length as well as across the member sections. The advanced analysis for steel frame design, proposed by the authors, is based on the spring-in-series model. The effect of joint semi-rigidity and partial strength is taken care of by specifying certain values of the initial stiffness, ultimate moment and the shape factor of the moment-rotation characteristic for the spring representing the joint. The effect of imperfections affecting the performance of imperfect structural members in compression is modelled by the application of a simplified tangent modulus concept combined with the reduction of the initial value of the elasticity modulus. The effect of residual stresses is taken care of by specifying certain values of the shape parameter for the moment-rotation characteristic of the spring representing the gradual yielding of the member. It is dependent upon the cross-section type and fabrication method (ie upon the residual stress pattern resulting from rolling or welding processes). A case study analysis is presented. Concluding remarks referring to the application of advanced analysis in design, pertaining to the study case considered, are drawn.

Keywords: steel frame, semi-rigid joint, advanced analysis, spring-in-series model.

1. Introduction

Over the past 25 years, extensive research has been made to develop and validate several advanced analysis methods that can capture the frame ultimate strength through the geometrically and materially non-linear analysis carried out in such a way that member local and overall buckling capacity checks are not required. Second order plastic-zone, conventional plastic-hinge and refined plastic-hinge methods may be used in advanced analysis. These methods differ as to the degree of refinements in representing the plastic yield effects of joints and members. The plastic zone method allows for the detailed modelling of the gradual yielding effects across the member sections and along the member length, in contrast to the conventional plastic-hinge method. The latter one does not allow for any refinements since a rigid-perfectly-plastic relationship for the behaviour of member sections and an elastic-perfectly-plastic relationship for the behaviour of joints are used. The refined plastic-hinge method is somewhere in between the two above-mentioned methods but it may be calibrated in such a way that it reproduces, with the accuracy acceptable for practical application, the behaviour of real structures (ie imperfect structures).

Refined plastic-hinge methods for advanced frame analysis are based on different assumptions used in modelling the stiffness degradation effects. Two methods gained popularity, namely the method based on a two-surface degradation model [1] and the method based on a spring-in-series model [2]. In the former advanced analysis, two element end springs representing the joint flexibility are used and combined with the introduction of two stiffness reduction factors representing the effect of member inelastic deformations. The reduction factors are applied directly to flexural terms of the element stiffness matrix. In the latter method of advanced analysis, two-element end springs are used in order to represent the effects of joint flexibility and member yielding. This method is further developed by the authors in order to account for the effect of imperfections on the behaviour of structural systems.

A brief summary of the spring-in-series model is followed by the detailed discussion of issues related to the influence of imperfections on the frame load deflection characteristic and the frame ultimate state. The proposed values of model parameters are verified. The example of a sway frame is considered in order to show how the different values of model parameters affect the

frame load deflection characteristic, the ultimate load capacity and the magnitude of deflection at the frame ultimate state. Final conclusions are drawn.

2. Implementation of the spring-in-series model

Let us consider a finite element (FE) of discretised structure, consisting of the member with two springs at each node and subjected to flexural deformations only [2]. The arrangement of components in this finite element is depicted in Fig 1. The finite element representation of the incremental equilibrium equations in the local co-rotational coordinates can be summarised as follows

$$\Delta\mathbf{Q} = \left(\mathbf{k_{j1}} + \mathbf{k_{m1}} + \mathbf{k} + \mathbf{k_{m2}} + \mathbf{k_{j2}}\right)\Delta\mathbf{q}\,, \qquad (1)$$

where the set of equations (1) is expressed in terms of internal and external static and kinematic variables, associated with the member nodes, joint nodes and finite element nodes. All the node types are given in Fig 1, with reference to the origin (denoted by 1) and the end (denoted by 2).

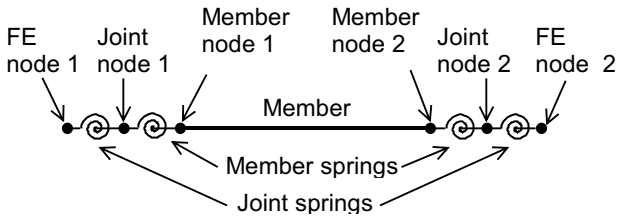

Fig 1. Finite element with internal degrees of freedom

The incremental nodal forces and displacements in equation (1) are expressed as follows:

$$\Delta\mathbf{Q} = \begin{bmatrix} \Delta M_1 \\ \Delta M_{j1} \\ \Delta M_{m1} \\ \Delta M_{m2} \\ \Delta M_{j2} \\ \Delta M_2 \end{bmatrix}, \quad \Delta\mathbf{q} = \begin{bmatrix} \Delta\varphi_1 \\ \Delta\phi_{j1} \\ \Delta\phi_{m1} \\ \Delta\phi_{m2} \\ \Delta\phi_{j2} \\ \Delta\varphi_2 \end{bmatrix}, \qquad (2)$$

where $\Delta\varphi_1, \Delta\varphi_2$ – finite element degrees of freedom (external DOFs), $\Delta\phi_{j1}, \Delta\phi_{j2}$ – joint spring degrees of freedom (internal DOFs), $\Delta\phi_{m1}, \Delta\phi_{m2}$ – member spring degrees of freedom (internal DOFs).

The components of the finite element stiffness matrix in equation (1) are expressed as follows:
– the contribution of the joint instantaneous stiffness at the origin:

$$\mathbf{k_{j1}} = S_{j1}\begin{bmatrix} 1 & -1 & 0 & 0 & 0 & 0 \\ -1 & 1 & 0 & 0 & 0 & 0 \\ 0 & 0 & 0 & 0 & 0 & 0 \\ 0 & 0 & 0 & 0 & 0 & 0 \\ 0 & 0 & 0 & 0 & 0 & 0 \\ 0 & 0 & 0 & 0 & 0 & 0 \end{bmatrix} \qquad (3)$$

– the contribution of the joint instantaneous stiffness at the end;

$$\mathbf{k_{j2}} = S_{j2}\begin{bmatrix} 0 & 0 & 0 & 0 & 0 & 0 \\ 0 & 0 & 0 & 0 & 0 & 0 \\ 0 & 0 & 0 & 0 & 0 & 0 \\ 0 & 0 & 0 & 0 & 0 & 0 \\ 0 & 0 & 0 & 0 & 1 & -1 \\ 0 & 0 & 0 & 0 & -1 & 1 \end{bmatrix} \qquad (4)$$

– the contribution of member imperfections and plastic zones developing from the origin onward;

$$\mathbf{k_{m1}} = S_{m1}\begin{bmatrix} 0 & 0 & 0 & 0 & 0 & 0 \\ 0 & 1 & -1 & 0 & 0 & 0 \\ 0 & -1 & 1 & 0 & 0 & 0 \\ 0 & 0 & 0 & 0 & 0 & 0 \\ 0 & 0 & 0 & 0 & 0 & 0 \\ 0 & 0 & 0 & 0 & 0 & 0 \end{bmatrix} \qquad (5)$$

– the contribution of member imperfections and plastic zones developing from the end backward;

$$\mathbf{k_{m2}} = S_{m2}\begin{bmatrix} 0 & 0 & 0 & 0 & 0 & 0 \\ 0 & 0 & 0 & 0 & 0 & 0 \\ 0 & 0 & 0 & 0 & 0 & 0 \\ 0 & 0 & 0 & 1 & -1 & 0 \\ 0 & 0 & 0 & -1 & 1 & 0 \\ 0 & 0 & 0 & 0 & 0 & 0 \end{bmatrix} \qquad (6)$$

– and finally, the contribution of the member elastic stiffness with the second-order effects taken into account;

$$\mathbf{k} = \frac{EI}{L}\begin{bmatrix} 0 & 0 & 0 & 0 & 0 & 0 \\ 0 & 0 & 0 & 0 & 0 & 0 \\ 0 & 0 & k_{11} & k_{12} & 0 & 0 \\ 0 & 0 & k_{21} & k_{22} & 0 & 0 \\ 0 & 0 & 0 & 0 & 0 & 0 \\ 0 & 0 & 0 & 0 & 0 & 0 \end{bmatrix} \qquad (7)$$

The terms of the member elastic stiffness component given by equation (7) are written in the standard form:

$$k_{11} = k_{22} = 4 + \frac{2}{15}\lambda^2\,, \quad k_{12} = k_{21} = 2 - \frac{1}{30}\lambda^2\,, \qquad (8)$$

where the member axial load factor

$$\lambda^2 = \frac{NL^2}{EI}, \tag{9}$$

and: N – the member axial force, L – the element length, E – Young modulus, I – sectional moment of inertia.

The contribution of the joint stiffness is evaluated on the basis of joint tangent stiffnesses S_{j1} (calculated for the spring placed at the origin) and S_{j2} (calculated for the spring placed at the end). They depend upon the magnitude of total moments in the current incremental stage $M_{j1}=M_1$ and $M_{j2}=M_2$, respectively. Adopting the Kishi-Chen power model for the modelling of the stiffness degradation process [1], the joint tangent stiffness S_j can be expressed as follows:

$$S_j = S_{j,ini}\left[1-\left(\frac{M_j}{M_{j,R}}\right)^{n_j}\right]^{\frac{n_j+1}{n_j}}, \tag{10}$$

where the joint properties are: $S_{j,ini}$ – initial stiffness, $M_{j,R}$ – ultimate moment, n_j – shape factor of the moment-rotation characteristic accounting for the effect of joint gradual yielding.

The contribution of the member imperfections affecting the flexural behaviour and plastic zones is evaluated on the basis of tangent stiffnesses S_{m1} (calculated for the spring placed at the origin) and S_{m2} (calculated for the spring placed at the end). They depend upon the magnitude of total moments in the current incremental stage $M_{m1}=M_1$ and $M_{m2}=M_2$, respectively. In order to describe this effect, the Kishi-Chen power model is also adopted, so that the tangent stiffness S_m can be expressed in the way similar to equation (10):

$$S_m = S_{m,ini}\left[1-\left(\frac{M_m}{M_{m,R}}\right)^{n_m}\right]^{\frac{n_m+1}{n_m}}, \tag{11}$$

where the spring properties are: $S_{m,ini}$ – initial stiffness representing the effect of geometric imperfections, $M_{m,R}$ – ultimate moment of the member section (if necessary reduced in the presence of a non-zero axial force), n_m – shape factor of the moment-rotation characteristic accounting for the effect of residual stresses.

Recognising that $\Delta M_{j1} = \Delta M_{m1} = \Delta M_1$ and $\Delta M_{j2} = \Delta M_{m2} = \Delta M_2$, and condensing the set of equations (1) in order to eliminate internal degrees of freedom, the following condensed set of equations for the finite element, referred from here on to as the finite superelement (FSE), is obtained:

$$\Delta\mathbf{Q}_\varphi = \mathbf{k}_{T\varphi}\Delta\mathbf{q}_\varphi, \tag{12}$$

where the tangent stiffness matrix

$$\mathbf{k}_{T\varphi} = \frac{EI}{L}\begin{bmatrix} k_{T\varphi 11} & k_{T\varphi 12} \\ symm. & k_{T\varphi 22}\end{bmatrix} \tag{13}$$

and the condensed vectors of nodal forces and displacements

$$\Delta\mathbf{Q}_\varphi = \begin{bmatrix}\Delta M_1 \\ \Delta M_2\end{bmatrix}, \quad \Delta\mathbf{q}_\varphi = \begin{bmatrix}\Delta\varphi_1 \\ \Delta\varphi_2\end{bmatrix}. \tag{14}$$

The terms of the stiffness matrix in equation (12) can be expressed as

$$k_{T\varphi 11} = \frac{3\left\{k_{11}[3r_2+(1-r_2)k_{22}]-(1-r_2){k_{12}}^2\right\}r_1}{[3r_1+(1-r_1)k_{11}][3r_2+(1-r_2)k_{22}]-(1-r_1)(1-r_2){k_{12}}^2}, \tag{15}$$

$$k_{T\varphi 22} = \frac{3\left\{k_{22}[3r_1+(1-r_1)k_{11}]-(1-r_1){k_{12}}^2\right\}r_2}{[3r_1+(1-r_1)k_{11}][3r_2+(1-r_2)k_{22}]-(1-r_1)(1-r_2){k_{12}}^2}, \tag{16}$$

$$k_{T\varphi 12} = \frac{9k_{12}r_1r_2}{[3r_1+(1-r_1)k_{11}][3r_2+(1-r_2)k_{22}]-(1-r_1)(1-r_2){k_{12}}^2}. \tag{17}$$

The fixity factors in equations (15)-(17) are calculated on the basis of the spring-in-series model. Fig 2 shows the finite superelement after the condensation process.

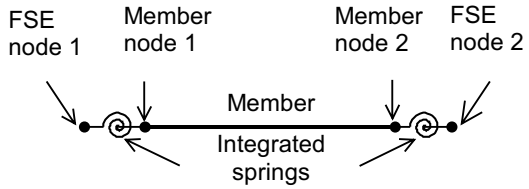

Fig 2. Finite superelement with external degrees of freedom

Two springs at each member end are integrated into one spring that has the integrated spring properties given by:

– tangent stiffnesses

$$S_1 = \frac{1}{\frac{1}{S_{j1}}+\frac{1}{S_{m1}}}, \tag{18}$$

$$S_2 = \frac{1}{\frac{1}{S_{j2}}+\frac{1}{S_{m2}}} \tag{19}$$

– ultimate moments

$$M_{R,1} = \min\left(M_{j,R1}; M_{m,R1}\right), \tag{20}$$

$$M_{R,2} = \min\left(M_{j,R2}; M_{m,R2}\right). \tag{21}$$

Thus the fixity factors

$$r_1 = \frac{1}{1+\frac{3EI}{S_1L}}, \quad r_2 = \frac{1}{1+\frac{3EI}{S_2L}}. \tag{22}$$

By the transformation of the set of equations (12) in order to express it in the coordinates associated with

the last known configuration and adding the contribution of the axial deformations, the final set of finite element local equations can be established. It has to be noted that the vectors of nodal forces and displacements of the final set of equations are referred to the external nodes of the superelement (nodes of the discretised structure). This is a set of equations for the element with the single spring at each node but with the integrated stiffnesses incorporated as a result of member and joint inelastic deformations, with the influence of imperfections taken into account.

3. Adopted solution procedure

Solution procedures for frame non-linear equilibrium equations can be one of the following:
– incremental-iterative methods that satisfy equilibrium equations at each incremental step of analysis, thus they allow to trace the equilibrium path accurately (within the degree of accuracy made possible by assumptions adopted in modelling),
– simple incremental methods that do not iterate for the equilibrium position at incremental steps, hence they produce a drift-off error in the prediction of the frame load deflection characteristic.

For practical applications, the simple incremental method is preferred since it is straightforward, it posesses the computational efficiency and, what is the most important, it can be treated as a natural extension of the linear analysis into the region of structural non-linear behaviour [1]. The computer implementation of advanced analysis presented herein is therefore based on the simple incremental procedure with a prescribed increment of the applied loads. In this procedure, at each incremental step, the values of member nodal forces and displacements are computed as sum of the incremental values. The entries to the stiffness matrix from each superelement are updated at the end of current increment, and only then a new load increment is applied. Fig 3 shows how the integrated spring properties are updated from the incremental step i to the next step $(i+1)$. The tangent stiffnesses of separate springs S_{ji} and S_{mi} are calculated on the basis of the total moments $M_{ji}= M_{mi}= M_i$. The stiffness S_i of the integrated spring in the step i is calculated according to (18) or (19), depending on the end number taken into consideration. The resultant stiffness S_i is kept constant for the incremental step $(i+1)$. The axial force entry to the superelement stiffness matrix is also updated and the axial force N_i from the step i used for the prediction of incremental forces and displacements in the step $(i+1)$. When under the constant load increment the force state exceeds that resulting from the ultimate moments (20) or (21), depending on the end number taken into consideration, a suitable scaling scheme is used to calculate the reduced load increment in order to avoid plastic hinges from forming within a constant-stiffness load increment (see Fig 3). Load step sizes less then or equal to the prescribed constant-stiffness load increment magnitude are computed directly, since the relations within the incremental step are linear. This is combined with a suitable search procedure for the formation of multiple hinges at one incremental step. Plastic hinges may therefore form only after the load increment.

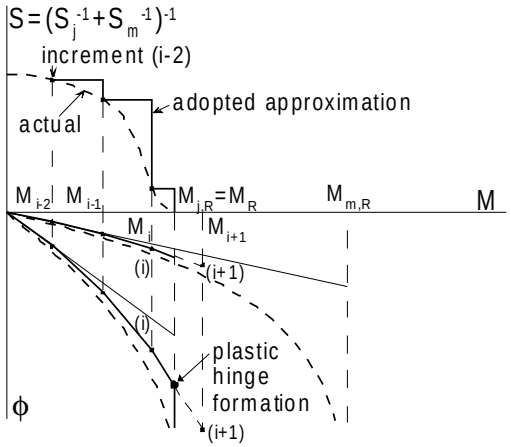

Fig 3. Constant-stiffness load increment scheme

4. Calibration of model parameters

4.1. Stiffness degradation in compression and tension

The axial force may have a great impact on the flexural stiffness of members. The P-δ effect is taken care of by the introduction of second-order terms in defining the flexural stiffness of the member element – see equations (8). The effect of imperfections on member inelastic deformations, such as residual stresses and out-of-straightness, is not explicitly reflected in equilibrium equations summarised in Chapter 3. The concept of tangent modulus was used in [1] for modelling the buckling behaviour of members in tension and compression. A similar concept is adopted for the advanced analysis proposed in this paper so that the Young modulus E is replaced in equation (13) by the tangent modulus E_T. The tangent modulus is constructed for a hypothetically ideal member in such a way that in case of compression it reproduces the behaviour of imperfect strut through the buckling curves of design specifications. The following formula is adopted

$$E_T = E_0\left[1-\left(\frac{N}{N_R}\right)^n\right]^{\frac{n+1}{n}}, \qquad (23)$$

where E_0 – reduced elasticity modulus representing the effect of geometric imperfections for compression of slender members (for tension members E_0=E), N_R – compression or tension capacity of the section, n – shape factor modelling the effect of residual stresses σ_r on the stress-strain curve of the axially loaded member.

The tangent modulus given by equation (23) reproduces the buckling resistance $N=N_{Rb}$ through the equation

$$\frac{N_{Rb}}{N_R} = \frac{1}{\bar{\lambda}^2}\frac{E_T}{E_0}, \tag{24}$$

where: $\bar{\lambda}$ – compression member relative slenderness ratio

$$\bar{\lambda} = \frac{\lambda}{\pi}\sqrt{\frac{N_R}{E_0 A}}, \tag{25}$$

and: λ – member slenderness, A – cross-sectional area.

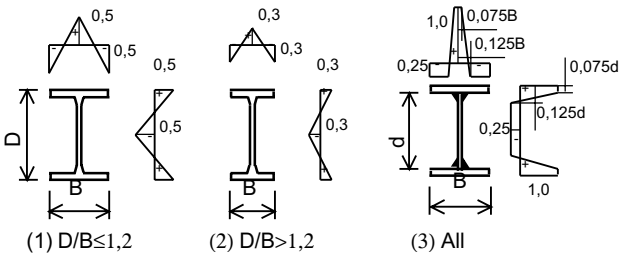

Fig 4. Standard residual stress patterns

The shape parameter, reflecting the effect of residual stresses σ_r, depends on the type of the cross-section. Generally three different types of I-sections and associated with them standard residual stress patterns are used (σ_r/f_y in Fig 4). For sections bent about the stronger axis, the buckling curve is taken from Table 1[3].

Table 1. Buckling curves for typical I-sections

Technology	Heat treatment	D/B >1,2	D/B ≤1,2
Rolled	–	*a*	*b*
Welded	Not-heat-treated	*a*	
	Annealed	*b*	

An exercise is carried out to find the best-fit shape parameters n for curves *a* and *b*. They are found to be n = 4 and n = 3 for curves *a* and *b* respectively. The effect of geometrical imperfections on the stiffness of compression members is approximately taken care of in such a way that the reduced elasticity modulus is calculated as the Young modulus divided by the partial safety factor γ_c applied to the buckling resistance of slender members. In [1] the value $1/\gamma_c = 0{,}85$ is suggested. The Polish code [3] uses for design values of the buckling resistance $1/\gamma_c = 0{,}75$. The European pre-code [4] uses $1/\gamma_c = 0{,}91$. If the reference is made do the American LRFD code [5], one can find out that the value of $1/\gamma_c = 0{,}877 \cdot 0{,}85 = 0{,}75$ is used. This agrees with the recommendations of the Polish code [3].

It is worth noting that the method of reduced elasticity modulus is a very convenient method to account for the effect of geometrical imperfections, if compared with the method of explicit imperfection modelling or the equivalent notional load method [1]. If the latter two methods are used, all the members have the elasticity modulus E, regardless whether they are under tension or compression.

4.2. Stiffness degradation in bending

Chen and Chui [2] proposed the following stiffness degradation relationship for the member spring

$$S_m = \infty \quad \text{for} \quad \frac{M}{M_{m,pr}} < \frac{M_{m,er}}{M_{m,pr}}, \tag{26}$$

$$S_m = \frac{6EI}{L}\frac{1-\dfrac{M}{M_{m,pr}}}{\dfrac{M}{M_{m,pr}}-\dfrac{M_{m,er}}{M_{m,pr}}} \quad \text{for} \quad \frac{M_{m,er}}{M_{m,pr}} \le \frac{M}{M_{m,pr}} \le 1, \tag{27}$$

where $M_{m,pr}$ – plastic moment of the cross section in the presence of axial force, $M_{m,er}$ – first yield moment, reduced in the presence of residual stresses, given by

$$M_{er} = \left(1 - \frac{\sigma_r}{f_y} - \frac{N}{N_R}\right) Z f_y, \tag{28}$$

and: Z – elastic section modulus, f_y – yield stress, σ_r – maximum value of the residual stress coordinate that for the standard cases can be taken from Fig 4.

In the computer implementation of the advanced analysis developed in [2], a very large value of 10^{+10} EI/L was assigned in the elastic region – equation (26), and a very small value of 10^{-10} EI/L in the post-yield region (when $M = M_{m,pr}$). The model is therefore somewhat complicated since is based on a discontinuous relationship, requiring artificial numbers to be used for avoiding numerical difficulties.

A different model is developed for the proposed advanced analysis. The effect of stiffness degradation in bending is taken care of by the adoption of equation (10). The model parameters are calibrated against the Chen-Chui proposal [2] for the case of pure bending. When integrating equations (26) and (27), the following section spring moment-rotation characteristic is obtained

$$\phi = 0 \quad \text{for} \quad \frac{M}{M_{m,pr}} < \frac{M_{m,er}}{M_{m,pr}}, \tag{29}$$

$$\phi = \frac{M_{m,pr}L}{6EI}\left\{\left(1-\frac{M}{M_{m,pr}}\right) - \left(1-\frac{M_{m,er}}{M_{m,pr}}\right)\times \left[1+\ln\left(1-\frac{M_{m,er}}{M_{m,pr}}\right)-\ln\left(1-\frac{M}{M_{m,pr}}\right)\right]\right\}$$

$$\text{for} \quad \frac{M_{m,er}}{M_{m,pr}} \le \frac{M}{M_{m,pr}} \le 1. \tag{30}$$

The average values of section plastic reserve shape factors $\alpha_p = S/Z$, where S is the section plastic modulus for bending about the strong axis, and the maximum residual stress factors $\overline{\sigma_r} = \sigma_r / f_y$ are used in the calibration (Table 2).

Table 2. Parameters used in calibration

Technology	Parameter	Section proportioning	
		D/B≤1,2	D/B>1,20
Rolled	α_p	1,10	1,15
	$\overline{\sigma_r}$	0,50	0,30
Welded	α_p	1,20	
	$\overline{\sigma_r}$	1,00	

The initial stiffness representing the effect of geometric imperfections (both out-of-flatness of sectional walls and member out-of-plane) are taken into consideration assuming the value of ten times greater than the stiffness multiplier in equation (27)

$$S_{m,ini} = \frac{60EI}{L}. \tag{31}$$

The lower-bound approximation is used for the calibration of shape factor n_m. It is chosen in such a way that the section spring moment-rotation characteristic of present formulation, for larger values of the rotation, approaches that proposed by Chen and Chui [2]. The values of n_m parameter are summarised in Table 3 and the resultant characteristics are compared in Fig 5 with those of Chen and Chui [2]. Numbers in brackets refer to the standard residual stress patterns given in Fig 4.

Table 3. Shape factors n_m of the moment-rotation characteristic

Technology	Section proportioning	
	D/B≤1,2	D/B>1,20
Rolled	(2) 1,25	(1) 1,60
Welded	(3) 0,75	

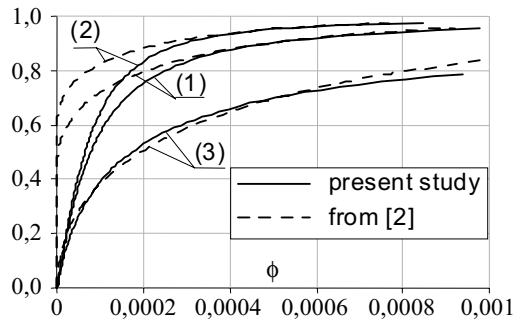

Fig 5. Comparison of section spring characteristics

4.3. Stiffness degradation of joints

The moment-rotation characteristic of joints adopted in the present study is of the same nature as the relationship for the modelling of member stiffness degradation in bending. The stiffness degradation in the adopted model is described by the continuous function – equation (9), which appears to be different from the approach recommended in European standardisation documents [4, 6]. The joint stiffness degradation used in [6] is a piecewise continuous function with the points of discontinuity at the levels of 2/3 of the ultimate moment and at the ultimate moment itself

$$S_j = S_{j,ini} \quad \text{for} \quad \frac{M}{M_{j,R}} < \frac{2}{3}, \tag{32}$$

$$S_j = S_{j,ini}\left(\frac{2}{3}\right)^{\psi} \frac{1}{(1+\psi)\left(\frac{M}{M_{j,R}}\right)^{\psi}}$$

$$\text{for} \quad \frac{2}{3} \le \frac{M}{M_{j,R}} \le 1, \tag{33}$$

$$S_j = 0 \quad \text{for} \quad \frac{\phi}{\phi_R} > 1, \tag{34}$$

where: ψ – parameter equal to 2,7 for end-plate joints and 3,1 for flange-cleated joints, and the rotation at the ultimate moment is given by

$$\phi_R = \left(\frac{3}{2}\right)^{\psi} \frac{M_{j,R}}{S_{j,ini}}. \tag{34}$$

The values of the joint stiffness at the discontinuity points are given in Table 4.

Table 4. Change in values of joint normalised stiffness

Point $M/M_{j,R}$	Change in $S_j/S_{j,ini}$	Joint type	
		End-plate	Flange-cleated
0,67	from	1,00	1,00
	to	0,27	0,24
1,00	from	0,09	0,07
	to	0,00	0,00

It can be noted from Table 4 that the parameter ψ does not have any impact on the stiffness degradation in end-plate and flange-cleated joints. In order to obtain an objective evaluation of the shape factor n_j of the proposed M-ϕ characteristic, and to maintain a similar reliability level as used in [6], the areas between the $S_j/S_{j,ini}$ curve from the European code [6] and that proposed herein are considered. The positive sign $A^{(+)}$ is assigned when the proposed curve lies below that from [6] and the negative sign $A^{(-)}$ in the opposite case. By considering the resultant parameter $\Delta A = A^{(+)} + A^{(-)}$, and predicting the value of n_j factor in such a way that

$\Delta A \cong 0$, the best fit solution is obtained. On the average of end-plate and flange-cleated joints, the value $n_j = 1{,}5$ is selected. The comparison of the joint M-ϕ characteristic adopted in the proposed advanced analysis and those from the European code [6] is given in Fig 6.

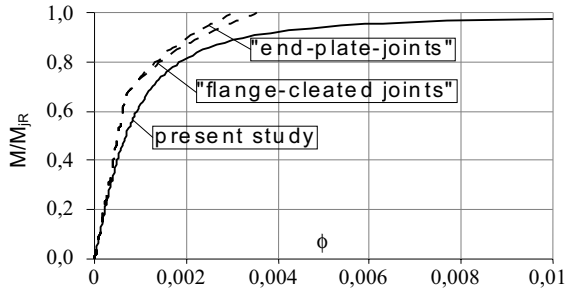

Fig 6. Comparison of joint M-ϕ characteristics

The joint physical parameters like initial stiffness and ultimate moment may be calculated by the component method given in [6]. The method requires the identification of the joint active components, calculation of the stiffness and strength of each component and finally the calculation of joint properties for the joint assembled from components. Since the procedure for calculating the joint physical properties is generally not friendly for hand calculations, the use of computer-based calculations is advisable [1, 7]. The proposed advanced analysis will be eventually based on the joint type catalogue from which the type of the joint can be identified and then its mechanical properties calculated automatically.

5. Computer programme and its applications

5.1. Computer code LILANN

The computer implementation of the proposed advanced analysis is based on the conventional geometrically linear plastic-hinge programme LILAN that has been used in engineering education at the Gdansk University of Technology and the University of Botswana (author C. J. Branicki [8]). This ensures that the programme LILANN being developed for the advanced analysis is of the same complexity as its predecessor. Thus, conventional plastic-hinge solving techniques and their numerical implementations for the geometrically non-linear analysis remain unchanged and may be applied within the refined plastic-hinge concept based on the spring-in-series model. Unlike other commercially available packages, the LILANN programme can be used with a great confidence by structural engineers who are familiar with the concepts and methods used in the programme because these concepts and methods have been taught during the university education.

The research version of the computer programm LILANN allows for the following analyses:
– **LL**: geometrically linear (first-order) analysis with bilinear joint characteristics,
– **NL**: geometrically non-linear (second-order) analysis with bilinear joint characteristics,
– **NN**: geometrically non-linear (second-order) analysis with curvilinear joint characteristics of Chen-Kishi type.

The analysis of type **NN** is to be finally implemented as advanced analysis for design purposes.

5.2. Frame for case study

In order to illustrate the differences between the application of analyses implemented in the research version of LILANN and the implication of different ways of modelling the geometric imperfections, the example of three-bay six-story frame shown in Fig 7 is considered.

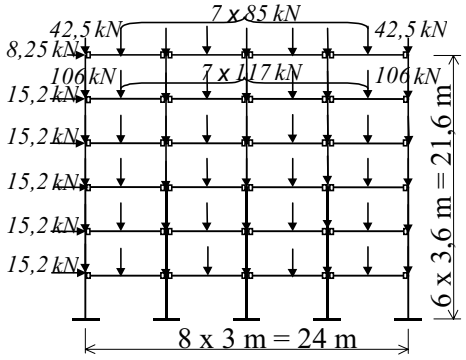

Fig 7. Frame geometry and loading

The unstiffened extended end-plate beam-to-column joints are used so that their semi-rigid partial-strength properties have to be considered in the frame analysis and design. Sizes of frame members as well as joint end-plate thicknesses and bolt diameters are taken the same as reported in [9]. The design was carried out automatically using the commercial package ROBOT Millennium. The options for elastic second-order analysis, non-linear joint M-ϕ characteristic and design according to the Polish steel code [3] were selected. Fig 8 shows the member sizes and the joint types yielding from the design.

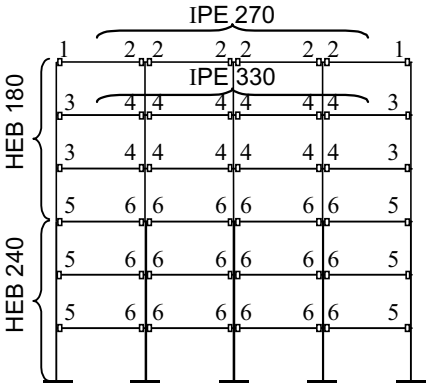

Fig 8. Member sizes and types of semi-rigid joints

The mechanical properties of beam-to-column joints are listed in Table 5.

Table 5. Mechanical properties of beam-to-column joints

Joint type	Connected profiles	Mechanical properties	
		Initial stiffness [kNm/rad]	Ultimate moment [kNm]
1	IPE 270 to HEB 180	16100	65
2	IPE 270 to HEB 180	54500	80
3	IPE 330 to HEB 180	25700	83
4	IPE 330 to HEB 180	84500	105
5	IPE 330 to HEB 240	31700	99
6	IPE 330 to HEB 240	79300	112

The classification of beam-to-column joints according to stiffness is conveniently done with use of the fixity factors. Fig 9 shows the bar graph for all the joints listed in Table 5. It is clear that joints have generally to be considered as semi-rigid. Examining the joint strength one can conclude that all the joints are of partial-strength.

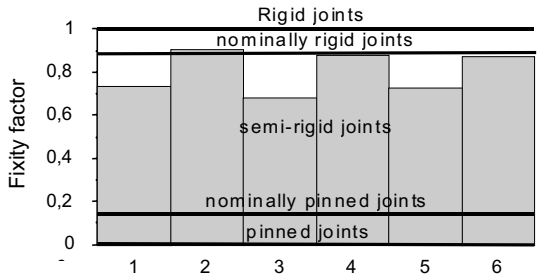

Fig 9. Classification of joints according to stiffness

The influence of geometric imperfections is simulated in such a way that three cases are considered using the following notations for types of analysis:

1) the modulus of elasticity of members with a compressive force is reduced to 0,85E and for members with a tensile and zero force kept E, while the notional horizontal loads are not added to the applied horizontal loads;

2) the modulus of elasticity of members with a compressive force is kept the same as for members with a tensile and zero force, and equal to E, while the notional horizontal loads are added to the applied horizontal loads;

3) the modulus of elasticity of members with a compressive force is reduced to 0,85E and for members with a tensile and zero force kept E, while the notional horizontal loads are also added to the applied horizontal loads.

5.3. Results of the analysis of LL type

Fig 10 shows the frame load deflection characteristics (the load factor vs the sway displacement of the frame top node) LL-1, LL-2 and LL-3, corresponding to three ways of modelling of geometric imperfections mentioned in the previous chapter. The results show that the ultimate load factor is the same for all the analyses. The difference occurs in displacements. The maximum displacement is for the analysis LL3, the smaller for the analysis LL-2 and the smallest for the analysis LL-1. The history of plastic hinge formation is shown in Fig 11 for the analysis LL-1, Fig 12 – for LL-2 and Fig 13 – for LL-3.

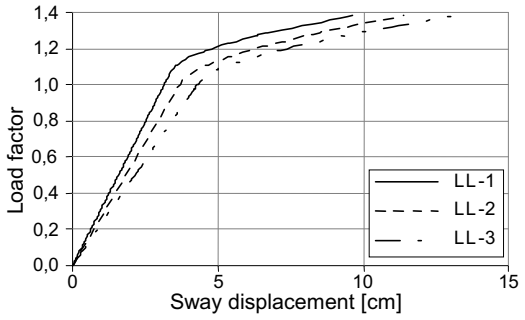

Fig 10. Load deflection characteristics for analyses LL

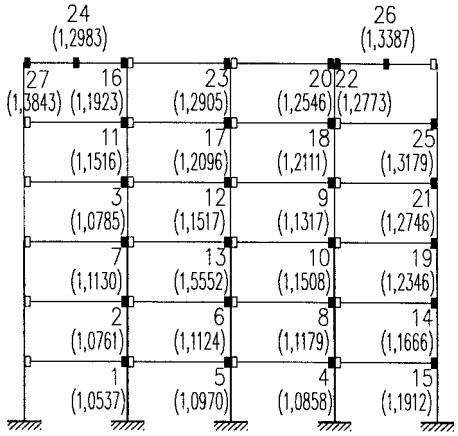

Fig 11. Plastic hinge formation history for analysis LL-1

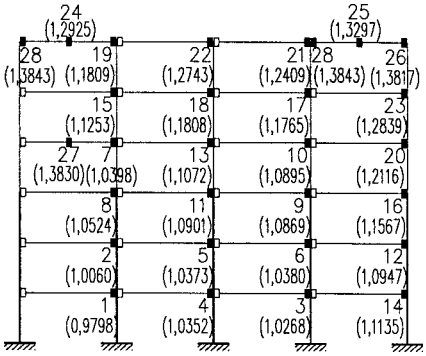

Fig 12. Plastic hinge formation history for analysis LL-2

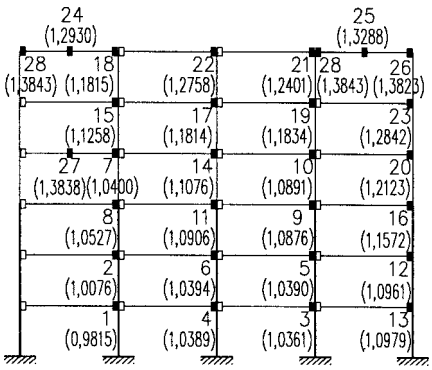

Fig 13. Plastic hinge formation history for analysis LL-3

5.4. Results of the analysis of NL type

Fig 14 shows the frame load deflection characteristics (the load factor vs the sway displacement of the top node of the frame) NL-1, NL-2 and NL-3, corresponding to three ways of modelling of geometric imperfections mentioned in Chapter 5.2.

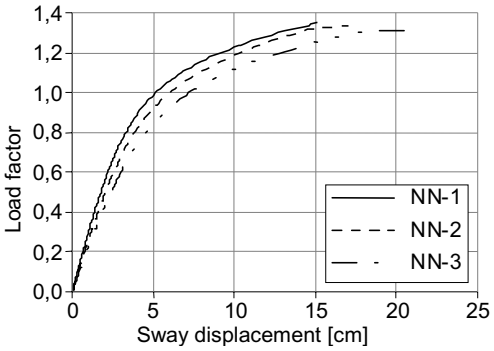

Fig 14. Load deflection characteristics for analyses NL

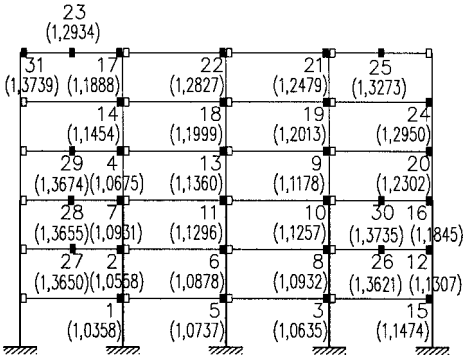

Fig 15. Plastic hinge formation history for analysis NL-1

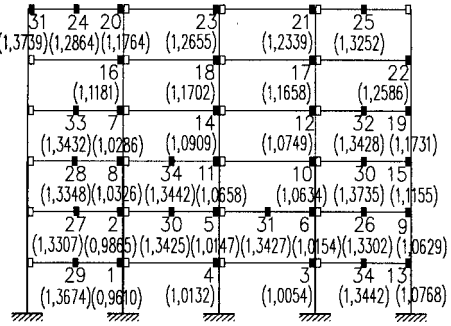

Fig 16. Plastic hinge formation history for analysis NL-2

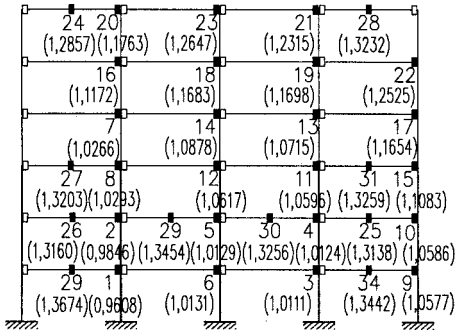

Fig 17. Plastic hinge formation history for analysis NL-3

The highest ultimate load factor is for the analysis NL-1, a lower for the analysis NL-2 and the lowest for the analysis NL-3. The difference occurs also in displacements. The maximum displacement is for the analysis NL3, the smaller for the analysis NL-2 and the smallest for the analysis NL-1. The history of plastic hinge formation is shown in Fig 15 for the analysis NL-1, Fig 16 – for NL-2 and Fig 17 – for NL-3.

5.5. Results from analysis of NN type

Fig 18 shows the frame load deflection characteristics (the load factor vs the sway displacement of the top node of the frame) NN-1, NN-2 and NN-3, corresponding to three ways of modelling the geometric imperfections mentioned in Chapter 5.2. The tendency in the ultimate load factor and in the considered displacement is the same as in the analysis of type NL. The history of plastic hinge formation is shown in Fig 19 for the analysis NN-1, Fig 20 – for NN-2 and Fig 21 – for NN-3.

6. Summary and concluding remarks

The conclusions drawn below pertain only to particular frame analysed in this paper. Summary of all the calculations is given in Table 6. For comparison, the results from PHINGE_R [10] are also provided so that one can see how the results change when different soft-

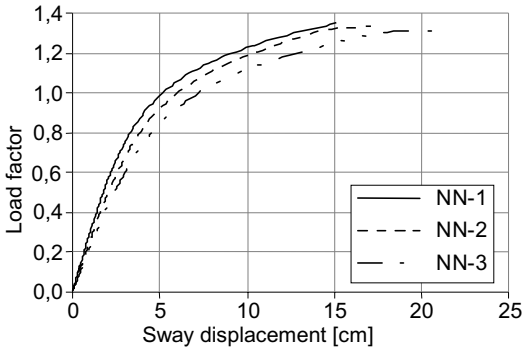

Fig 18. Load deflection characteristics for analyses NN

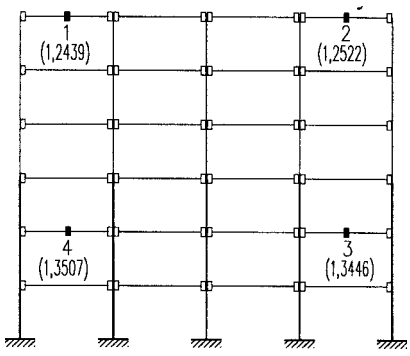

Fig 19. Plastic hinge formation history for analysis NN-1

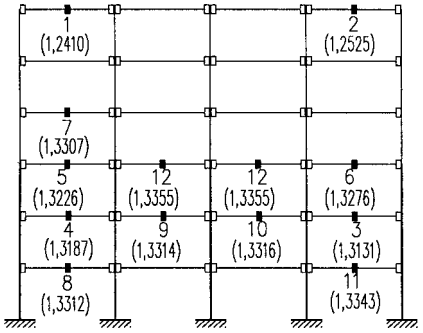

Fig 20. Plastic hinge formation history for analysis NN-2

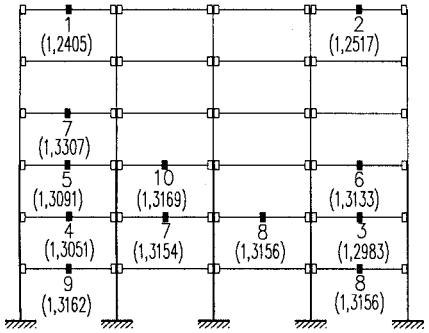

Fig 21. Plastic hinge formation history for analysis NN-3

ware is used. It can be concluded that though all analysis types predict ultimate load within a 4 % accuracy, the LL analyses predict the displacements that are 60 % underestimated. Since partial-strength joints are used, the member inelastic deformations may not be advanced in structural members so that the difference in results for NL and NN analyses is not observed. For the frame used in this study, both types of analysis may be recommended. When notional forces and the reduced elasticity modulus for elements with compression are used, the results are too conservative (results for NN-3 in Table 6). Comparing the results for analyses NN-1 and NN-2 one can see that the analysis NN-2 leads to the slightly lower load factor but of the meaningful higher displacements than the analysis NN-1.

The conclusion is that for achieving the same level of reliability in advanced analyses using notional loads or reduced elasticity modulus of structural members, a higher reduction of the elastic modulus of compression members is required. The suggestion is that the value close to that adopted in the American LRFD code [5] and in the Polish code [3] should be preferred for the frame considered. It implies that here the value $E_0 = 0{,}75E$ should be used instead of $E_0 = 0{,}85E$, as suggested for advanced analysis [1].

Table 6. Comparison of load factors and sway displacements

Software	Analysis type	Model type	Load factor	Sway [cm]
LILANN	LL	1	1,384	9,6
		2		11,4
		3		13,2
	NL	1	1,374	16,1
		2	1,344	16,7
		3	1,326	18,3
	NN	1	1,351	15,1
		2	1,336	17,1
		3	1,317	20,6
PHINGE_R	NN	1	1,331	10,8
		2	1,341	14,6
		3	1,346	17,1

The present study indicates a necessity for further research in order to calibrate model parameters for the proposed method in such a way that they reflect better the behaviour of real structures (imperfect structures).

References

1. Chen, W. F.; Kim, S. E. LRFD steel design using advanced analysis. Boca Raton & New York: CRC Press, 1997.
2. Chan, S. L.; Chui, P. P. T. Non-linear static and cyclic analysis of steel frames with semi-rigid connections. Amsterdam et al.: Elsevier, 2000.
3. PN-90/B-03200. Steel structures: Static calculations and design. Warsaw: PKNMiJ, 1990.
4. ENV 1993-1-1. Design of steel structures. Part 1: General rules and rules for buildings. Brussels: CEN, 1992.
5. AISC. Load and resistance factor design specifications. Chicago: American Institute of Steel Construction, 1994.
6. ENV 1993-1-8. Design of steel structures. Part 1.8–Design of joints. Brussels: CEN, 2001.
7. Fealla, C.; Pilusi, V.; Rizzano, G. Structural steel semi-rigid connections. Boca Raton & New York: CRC Press, 2000.
8. Branicki, C. J. LILAN: Program for plastic analysis of planar frames. CAL/CAT Structural analysis software. University of Gdansk-University of Botswana, 2002.
9. Brodka, J.; Barszcz, A.; Gizejowski, M. & Kozlowski A. Stiffness and strength of sway frames with semi-rigid joints. Rzeszow-Warszawa: Rzeszow Univ. Publishers, 2004 (in Polish) [in press].
10. Gizejowski, M. Computational models of steel plane frames with semi-rigid joints. Series: *Civil Engineering*, Vol 136. Warsaw: Warsaw University of Technology Press: Habil., 2000 (in Polish).